Journal of Advanced Ceramics
2017, **6**(2): 90–99
DOI: 10.1007/s40145-017-0221-9

ISSN 2226-4108
CN 10-1154/TQ

Research Article

Fabrication, mechanical properties, and tribological behaviors of Ti_2AlC and $Ti_2AlSn_{0.2}C$ solid solutions

Leping CAI[a], Zhenying HUANG[a,b,*], Wenqiang HU[a], Suming HAO[a], Hongxiang ZHAI[a], Yang ZHOU[a]

[a]*Centre of Materials Science and Engineering*, *School of Mechanical and Electronic Control Engineering*, *Beijing Jiaotong University*, *Beijing 100044*, *China*
[b]*Key Laboratory of Vehicle Advanced Manufacturing*, *Measuring and Control Technology* (*Beijing Jiaotong University*), *Ministry of Education*, *China*

Received: November 18, 2016; Revised: February 27, 2017; Accepted: March 08, 2017

Abstract: Highly pure and dense Ti_2AlC and $Ti_2AlSn_{0.2}C$ bulks were prepared by hot pressing with molar ratios of 1:1.1:0.9 and 1:0.9:0.2:0.85, respectively, at 1450 ℃ for 30 min with 28 MPa in Ar atmosphere. The phase compositions were investigated by X-ray diffraction (XRD); the surface morphology and topography of the crystal grains were also analyzed by scanning electron microscopy (SEM). The flexural strengths of Ti_2AlC and $Ti_2AlSn_{0.2}C$ have been measured as 430 and 410 MPa, respectively. Both Vickers hardness decreased slowly as the load increased. The tribological behavior was investigated by dry sliding a low-carbon steel under normal load of 20–80 N and sliding speed of 10–30 m/s. Ti_2AlC bulk has a friction coefficient of 0.3–0.45 and a wear rate of $(1.64–2.97)\times10^{-6}$ $mm^3/(N\cdot m)$, while $Ti_2AlSn_{0.2}C$ bulk has a friction coefficient of 0.25–0.35 and a wear rate of $(2.5–4.31)\times10^{-6}$ $mm^3/(N\cdot m)$. The influences of Sn incorporation on the microstructure and properties of Ti_2AlC have also been discussed.

Keywords: Ti_2AlC; $Ti_2AlSn_{0.2}C$; microstructure; mechanical property; tribological behavior

1 Introduction

Ternary compound MAX phase ceramics with nanolamellar structure have attracted more and more attention in recent years. The chemical general formula of MAX phase can be noted as $M_{n+1}AX_n$, where M is the transition metal element, A is the main IIIA or IVA group element, and X is C or N. For different value of n (n = 1, 2, 3), 211, 312, and 413 phases are synthesized. At present, there are more than 50 kinds of synthetic compounds, such as Ti_2SnC, Cr_2AlC, Ti_3AlC_2, Ti_4AlN_3, and so on [1–3]. Due to the similar layered structure and similar characteristics in the same location of different elements, the study of MAX phase solid solutions likewise aroused the interest of researchers [4–13]. In the existing researches, solid solutions like $(Cr_{1-x}V_x)_2AlC$ [4,5], $Ti_3Si(Al)C_2$ [6–8], $Ti_3Al(Sn)C_2$ [9–12], and $Ti_2AlC_{0.5}N_{0.5}$ [13] have been reported to possess improved flexural strength, hardness, tribological properties, thermal expansion coefficient, etc. MAX phases and their solid solutions are demonstrated to have considerable advantages of unique nanolamellar crystal structure, high strength, resistance to elevated temperature decomposition and chemical corrosion, and so on. Furthermore, these

* Corresponding author.
E-mail: zhyhuang@bjtu.edu.cn

compounds as well possess oxidation behaviors, high damage tolerance, resistance to thermal shock, and ductile-to-brittle transition, which are closely relevant to tribological properties [1,14–23]; therefore, they are promising candidates for tribological applications.

In recent ten years, many researches in tribological study of MAX phases like Ti_3SiC_2 and Ti_3AlC_2 and MAX matrix composite materials have been conducted [9,10,18–23]. Gonzalez-Julian *et al.* [19] consolidated the Cr_2AlC/SiC fiber composites to evaluate the tribological properties of Cr_2AlC, and found that the friction decreases up to 20% while the wear resistance increases up to 80% for Cr_2AlC/10SiC composite. The excellent mechanical performance of SiC fibers could account for the enhanced wear resistance. Gupta and Barsoum [21] chose Ta_2AlC, Ta_2AlC/Ag, and Cr_2AlC/Ag composites to test against Ni-based superalloys; they found out the tribological characteristics are mainly decided by the generated film of MAX phase or MAX matrix composite. Zhai *et al.* [22] and Huang *et al.* [23] reported that due to the oxide film with self-lubricating effect on the friction surface, Ti_3SiC_2 and Ti_3AlC_2 exhibit excellent tribological properties sliding against low-carbon steel. Xu *et al.* [9] and Huang *et al.* [10] added 0.2Sn and 0.4Sn to fabricate $Ti_3Al(Sn)C_2$ solid solutions; the experimental investigation showed that micro-Vickers hardness is about 12% higher and the flexural strength is increased by 51% and 67% respectively, compared with Ti_3AlC_2. Moreover, $Ti_3Al(Sn)C_2$ solid solutions showed excellent tribological properties during dry sliding against a low-carbon steel disk. The friction coefficient could be adapted to fall within the range of 0.1–0.4 after incorporation of different amounts of Sn to form $Ti_3Al(Sn)C_2$ solid solutions while retaining excellent wear resistance. The adjustable friction coefficient and excellent wear properties of $Ti_3Al(Sn)C_2$ solid solutions were mainly attributed to the formation of a self-adaptable friction oxide film which was composed of Ti, Sn, Al, and Fe oxide composition after the incorporation of different amounts of Sn. In Ref. [18], tribological behavior of Ti_3AlC_2 against SiC at ambient and elevated temperatures was studied by Ma *et al*. The friction coefficient and wear rate of Ti_3AlC_2 are very low at elevated temperatures. The compacted protective oxide layer on the worn surface is believed to be responsible for the quite low wear rate of Ti_3AlC_2. Ti_3AlC_2 has excellent oxidation resistance and retains decent mechanical properties at elevated temperature, and it has excellent promise as solid lubricant material due to the layered nature.

As a member of MAX phases, Ti_2AlC shows low density, high modulus, and excellent oxidation resistance, which can be applied in the adverse working condition of oxidation environment [15,16,24,25]. There have been some researches about the preparation and properties of Ti_2AlC. Lin *et al.* [24] used Ti, Al, and graphite elemental powders as raw materials and prepared Ti_2AlC bulk with lattice constants of $a = 0.304$ nm and $c = 1.36$ nm by an *in situ* hot pressing/solid–liquid reaction process, and the microstructural characterization of Ti_2AlC was carried out as well. Li *et al.* [25] reported that Ti_2AlC ceramic achieves at least seven healing cycles after repeated cracking at a given location. The main healing mechanism at high temperature is the filling of the cracks by the formation of well adhering α-Al_2O_3 and the presence of some AlO_2 rutile. Bei *et al.* [15] synthesized $Ti_2Al_{1-x}Sn_xC$ solid solution with Ti, Al, Sn, and TiC powders, and investigated the effect of incorporating Sn on the oxidation behaviors. They found that SnO_2 is formed at temperatures significantly lower than that of TiO_2 (rutile) and Al_2O_3 [15]. MAX phase $Ti_2Al_{1-x}Sn_xC$ solid solution is of interest to serve as a repair filler for oxidation-induced crack healing in ceramic matrix composites at temperatures below 1000 ℃ [15,16]. Up to now, there is few research about 211 phase of Ti_2AlC and $Ti_2AlSn_{0.2}C$ in tribological behaviors. Substitution of A element in Ti_2AlC phase solid solution by low-melting elements such as Sn may offer potential for different tribological applications. This paper mainly focused on the fabrication of pure Ti_2AlC and $Ti_2AlSn_{0.2}C$ solid solutions by hot pressing sintering method; the microstructure, mechanical properties, and the tribological behavior were analyzed as well. The effect of incorporating Sn on mechanical and tribological characteristics was also discussed by comparing with Ti_2AlC ceramic.

2 Experimental procedures

Powders of Ti (average particle size 48 μm, 99.5 wt% purity), Al (average particle size 75 μm, 99.5 wt% purity), Sn (average particle size 75 μm, 99.5 wt% purity), and TiC (average particle size 48 μm, 99.5 wt% purity) were used as starting materials. The designed molar ratios were Ti:Al:TiC = 1:1.1:0.9 for Ti_2AlC ceramic and Ti:Al:Sn:TiC = 1:0.9:0.2:0.85 for $Ti_2AlSn_{0.2}C$ ceramic. For both compositions, a little

excess Al and Sn were used to compensate for the loss of these elements by evaporation during the sintering process; a little deficient C was also introduced into the starting composition to obtain high-purity ceramics. The mixed powders were hot pressed at 1450 ℃ for 30 min with 28 MPa in Ar atmosphere to synthesize Ti_2AlC and $Ti_2AlSn_{0.2}C$ bulks.

The phase composition of the materials was identified by X-ray diffraction (XRD) analysis using a D/Max 2200 PC diffractometer operating with Cu Kα radiation at 40 kV and 40 mA. Microstructure of the phase was identified using a scanning electron microscope (SEM, ZEISSEVO18) equipped with an energy dispersive X-ray spectrometer (EDS, Bruker Nano XFlash detector 5010). The observed grain surface of bulks was polished and etched by the HF and HNO_3 mixed acid. The average grain sizes for the hot pressed Ti_2AlC and $Ti_2AlSn_{0.2}C$ samples were measured by the software named Nano Measurer. The Vickers hardness was determined with a TH700 hardness tester in a load range of 4.9–98 N with a dwell time of 15 s. The flexural strength was measured with 3 mm × 4 mm × 36 mm specimens using a three-point bending device with a crosshead speed of 0.5 mm/min and a span size of 30 mm.

The Ti_2AlC and $Ti_2AlSn_{0.2}C$ samples were cut into blocks of 10 mm × 10 mm × 12 mm. The samples were polished by 800 mesh sand paper. A low-carbon steel disk (containing 0.20% C, 0.40% Mn, 0.30% Si, ⩽0.2% Cr, and ⩽0.30% Ni) of ϕ300 mm × 10 mm was used as the friction counterpart. Friction and wear tests were performed on a block-on-disk-type tester at room temperature; the testing machine is illustrated in Fig. 1. The normal sliding contacting area between the block and the disk was 10 mm × 10 mm. The sliding speed was at a range of 10–30 m/s, and the applied normal load was in the range of 20–80 N. The sliding distance used for the continuous process was kept as 12,000 m. An adequate pre-abrasion was performed to make the normal friction surface of the block completely contact with the external surface of the disk. The pre-abrasion was also made whenever the test condition was changed to minimize possible influence of the speed- or load-relevant history on the friction surface condition. Tests were repeated three times for every given condition, and the average value was used as the evaluated data.

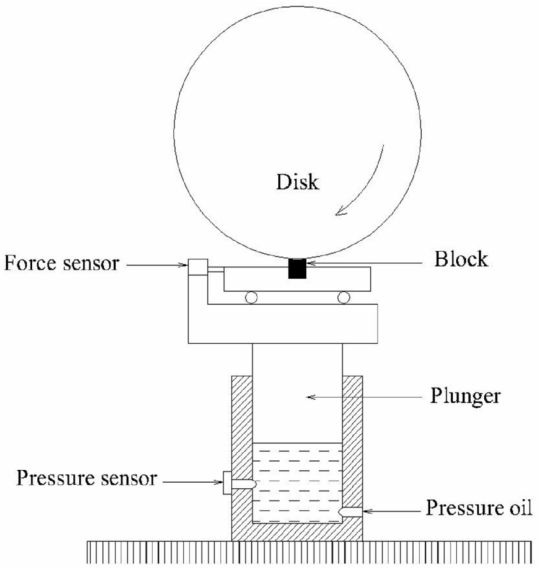

Fig. 1 Diagram of the block-on-disk-type friction testing machine.

3 Results and discussion

3.1 Phase composition and microstructure

The XRD patterns of Ti_2AlC and $Ti_2AlSn_{0.2}C$ bulks are shown in Fig. 2. From the diffraction pattern of Ti_2AlC, it can be seen a fraction of Ti_3AlC_2 impurity. Actually, in the process of the preparation of Ti_2AlC, Ti_3AlC_2 phase is difficult to eliminate [13,15]. These two phases can be generated from the following reactions: Ti + Al + TiC → Ti_2AlC, Ti + Al + 2TiC → Ti_3AlC_2. The sintering process of Ti_3AlC_2 is similar to that of Ti_2AlC; consequently it is difficult to suppress the generation of Ti_3AlC_2. No impurity phases, such as TiC, $TiAl_3$, Ti_6Sn_5, or Ti_5Sn_3, are detected in the XRD spectrum for $Ti_2AlSn_{0.2}C$. All diffraction peaks belonging to $Ti_2AlSn_{0.2}C$ are shifted slightly to the left compared with the lines of Ti_2AlC. The shift of diffraction peaks indicates dissolution of Sn into the A-element position of Ti_2AlC. The diffraction peaks belonging to (101) and

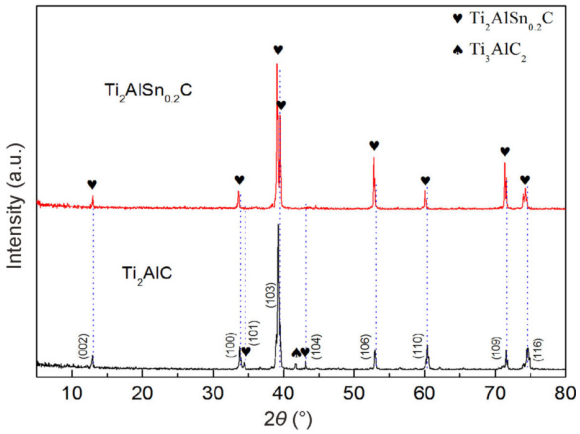

Fig. 2 XRD patterns for Ti_2AlC and $Ti_2AlSn_{0.2}C$ bulks.

(104) crystal planes almost do not exist in $Ti_2AlSn_{0.2}C$ solid solution.

The microstructures of Ti_2AlC and $Ti_2AlSn_{0.2}C$ bulks are shown in Fig. 3. Backscattered SEM image of a polished surface of Ti_2AlC shown in Fig. 3(a) reveals two phases: Ti_2AlC and a little amount of Ti_3AlC_2. The average chemical composition of Ti_2AlC as determined with EDS equals 51.2 at% Ti, 17 at% Al, 31.83 at% C, and the average chemical composition of Ti_3AlC_2 as determined with EDS equals 50.9 at% Ti, 21.16 at% Al, 27.93 at% C, in good agreement with that identified with the XRD patterns (shown in Fig. 2). Figure 3(b) shows the typical grain micrograph of Ti_2AlC (the observed surface was polished and etched by the HF and HNO_3 mixed acid, as well as Fig. 3(d)); most of the grains have a plate shape and a layered structure. The average size of the grains is estimated to be ~20 μm in length and ~8 μm in width. Observing the surface of $Ti_2AlSn_{0.2}C$ bulk in Fig. 3(c), there exists no other impurity phase; nevertheless, Al_2O_3 has been formed due to reaction of Al with oxygen that is present as an absorbed species at the original powder surface. A small amount of Al_2O_3 is commonly observed in Al-containing MAX phase, like $Ti_3Al(Sn)C_2$ [9,10] and $Cr_2Al(Si)C$ [17]. The grains of $Ti_2AlSn_{0.2}C$ are lined up tightly as shown in Fig. 3(d) and have the specific lamellar structure of MAX phase. The higher magnification SEM images are in the upper right corners of Figs. 3(b) and 3(d), and obvious layered structure can be observed. The average size of the $Ti_2AlSn_{0.2}C$ grains is estimated to be ~15 μm in length and ~5 μm in width, and the grain size is reduced slightly compared to the Ti_2AlC grains. The average chemical composition of $Ti_2AlSn_{0.2}C$ as determined with EDS equals 48.24 at% Ti, 17.78 at% Al, 5.94 at% Sn, 28.08 at% C; Al and Sn contents in the product are a little lower than expected on the basis of the mixture of powders prior to the synthesis of the ceramic, suggesting some of them were lost in the process of sintering. It turns out that the Sn dissolves into Ti_2AlC resulting in $Ti_2Al_{0.75}Sn_{0.25}C$.

3. 2 Mechanical properties

Table 1 listed the volume density, Vickers hardness, and flexural strength of Ti_2AlC and $Ti_2AlSn_{0.2}C$ in this work, and the Ti_2AlC and Ti_2SnC from other work are also listed for comparison. The volume density of Ti_2AlC is measured to be 4.1 g/cm^3, which is almost close to 4.06 g/cm^3 in Ref. [26]; the volume density of $Ti_2AlSn_{0.2}C$ is measured to be 4.6 g/cm^3, between the density values of Ti_2AlC and Ti_2SnC [27]. Under the load of 9.8 N, the Vickers hardness of Ti_2AlC is measured to be ~5.55 GPa, much higher than that of Ti_2AlC in Ref. [26]. After incorporation of 0.2Sn, the hardness of $Ti_2AlSn_{0.2}C$ (~3.92 GPa) solid solution has decreased by 30% compared with Ti_2AlC (~5.55 GPa),

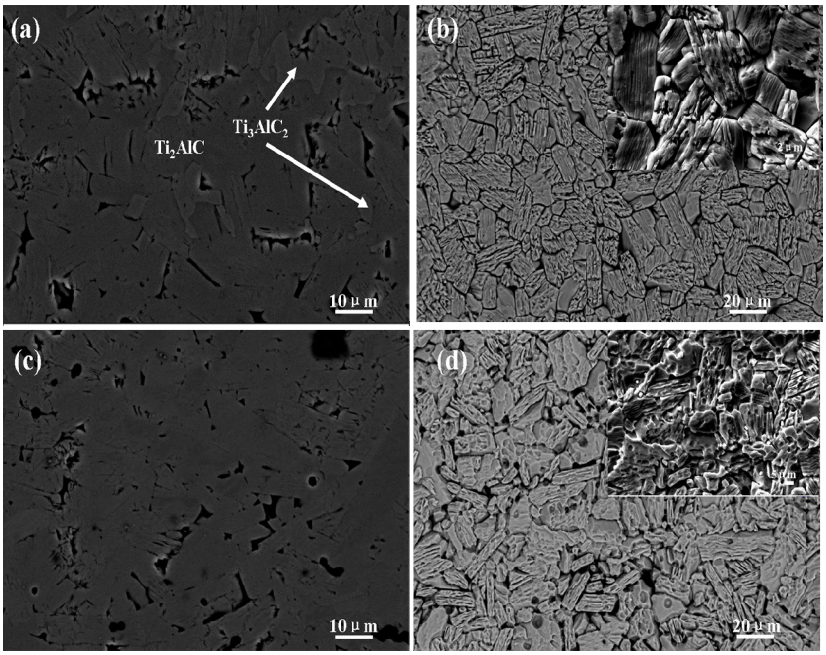

Fig. 3 SEM microstructures of (a, b) Ti_2AlC and (c, d) $Ti_2AlSn_{0.2}C$. The observed grain surfaces of bulks were polished and etched by the HF and HNO_3 mixed acid.

Table 1 Volume density, Vickers hardness, and flexural strength of Ti_2AlC, $Ti_2AlSn_{0.2}C$, and Ti_2SnC

Bulk	Volume density (g/cm^3)	Vickers hardness under the load of 9.8 N (GPa)	Flexural strength (MPa)	Reference
Ti_2AlC	4.1	5.55±0.69	430±32	This work
	4.06	3.5	261	[26]
$Ti_2AlSn_{0.2}C$	4.6	3.92±0.35	410±27	This work
Ti_2SnC	6.34	3.7	313	[27]

but this value is slightly higher than that of the single phase of Ti_2SnC [27]. The Vickers hardnesses of Ti_2AlC and $Ti_2AlSn_{0.2}C$ show a similar trend in the load range of 4.9–98 N (see Fig. 4), both gradually reducing with increase in load and approaching to 4 and 3 GPa, respectively, under the load of 98 N. The flexural strength of the Ti_2AlC bulk is about 430 MPa, much higher than that in Ref. [26]. And the flexural strength of $Ti_2AlSn_{0.2}C$ is measured to be 410 MPa, a little lower than that of Ti_2AlC bulk, but much higher than that of single-phase Ti_2SnC bulk in Ref. [27]. Both the hardness and flexural strength of the Ti_2AlC bulk are much higher than that in Ref. [26], maybe due to the higher density and existence of a little Ti_3AlC_2 in the material in this work. Ti_3AlC_2 is known to have decent mechanical properties. The distribution of Ti_3AlC_2 phase in Ti_2AlC plays the part of the dispersion strengthening effect. What is more, the average grain size of Ti_2AlC in this work is much smaller than that in Ref. [26], in which the crystallite size of Ti_2AlC is 41±12 μm in diameter and 16±4 μm in thickness. Existing research [28] shows that the fine-grained material exhibits higher strength compared with the coarse-grained materials. So the hardness and strength of Ti_2AlC obtained in this study are significantly higher than those reported in the same phase by others.

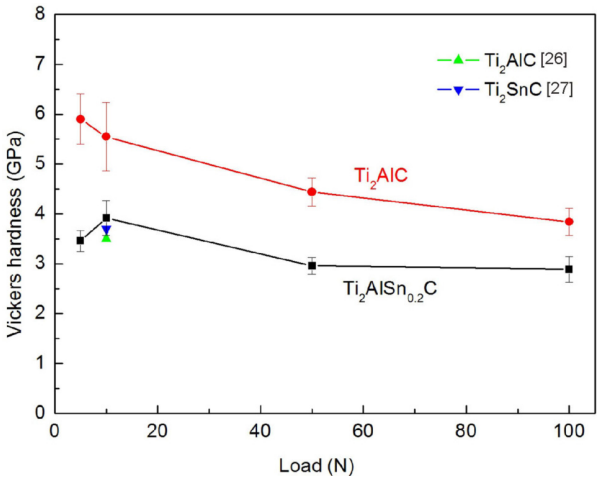

Fig. 4 Vickers hardness versus indentation load for Ti_2AlC and $Ti_2AlSn_{0.2}C$.

Figure 5 shows the SEM micrographs of damage modes in the fracture surfaces of Ti_2AlC and $Ti_2AlSn_{0.2}C$. The similar damage modes, such as grain delamination and kink band formation can be found on the fracture surface of Ti_2AlC (Figs. 5(a) and 5(b)) as well as on the fracture surface of $Ti_2AlSn_{0.2}C$ (Figs. 5(c) and 5(d)). However, for incorporation of 0.2Sn in Ti_2AlC bulk, the solid solution hardening and strengthening effect is not operative in this system. The same kind of results has been obtained in other 211 MAX phase, such as in $Cr_2Al(Si)C$ and $(Ti,Nb)_2AlC$ solid solutions [17,29]. By contrast, significant hardening and strengthening effect has been shown in that with substitution into A site of 312 MAX phase [7–10]. Zhou *et al.* [7] showed that flexural strength and microhardness of $Ti_3Al_{0.75}Sn_{0.25}C_2$ solid solution are enhanced by 12% and 26%, respectively, compared with those of single-phase Ti_3AlC_2. Li *et al.* [8] measured the flexural strength of $Ti_3SiAl_{0.2}C_2$ to be 425 MPa, 13% above that of Ti_3AlC_2. In our earlier work [9,10], the microhardness and flexural strength of the $Ti_3SiAl_{0.2}C_2$ solid solution were measured to be 3.53 GPa and 560 MPa, respectively, and the value is 12% and 51% higher than that of Ti_3AlC_2. However, the exact mechanism of strengthening or weakening effect of the MAX solid solution by substitution into A site is uncertain now. Actually our existing experimental results are not enough to explain the problem, and more work needs to be done, such as adding more content of Sn to prepare $Ti_2Al_{1-x}Sn_xC$ ($x = 0$–1) solid solution, to understand the influence of Sn in mechanical properties. This work is under performed.

3.3 Tribological characteristics

The friction coefficient and wear rate changes of Ti_2AlC and $Ti_2AlSn_{0.2}C$ with normal load under different sliding speed against low-carbon steel are shown in Fig. 6. In the normal load range of 20–80 N, the friction coefficient of Ti_2AlC decreases with increase in the sliding speed. In addition, for different sliding speeds, the friction coefficient seldom relies on normal load, always maintaining within a narrow range. At the sliding speed of 10, 20, and 30 m/s, the friction coefficient remains around 0.45, 0.35, and 0.3, respectively. Compared with Ti_2AlC, the importation of 0.2Sn (see Fig. 6(b)) results in a slight decrease in the friction coefficient, keeping at 0.35, 0.33, and 0.25, respectively. Additionally, the friction coefficient grows more stable for $Ti_2AlSn_{0.2}C$.

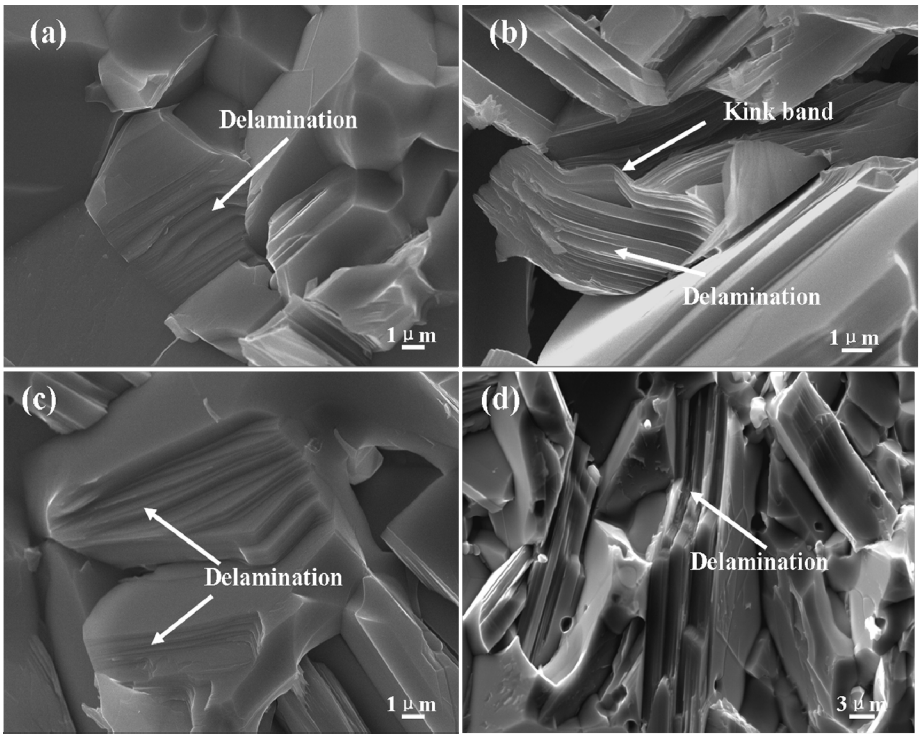

Fig. 5 SEM micrographs of the damaged modes observed in fracture surfaces of (a, b) Ti_2AlC and (c, d) $Ti_2AlSn_{0.2}C$.

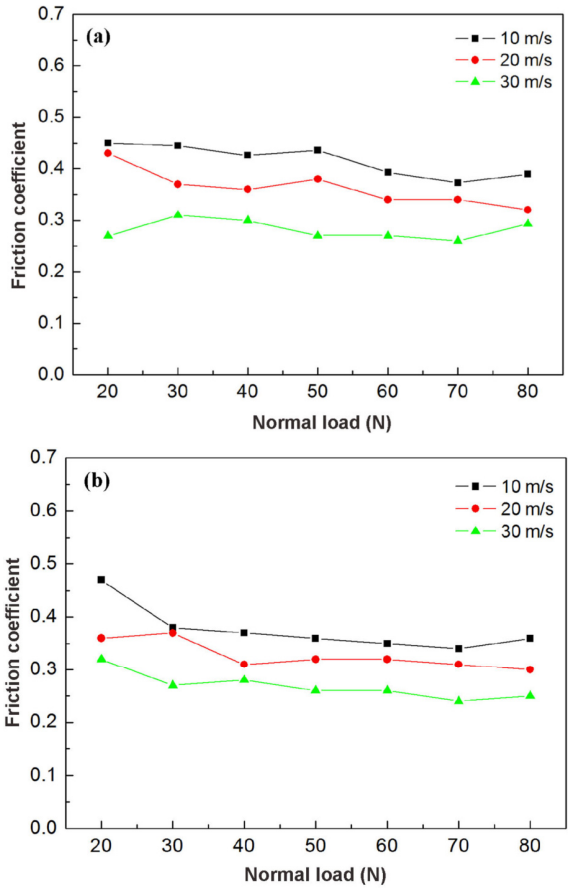

Fig. 6 Friction coefficients of (a) Ti_2AlC and (b) $Ti_2AlSn_{0.2}C$ sliding against low-carbon steel at different sliding speeds as a function of normal load.

The function curve of wear rate at different sliding speeds and normal loads of Ti_2AlC is shown in Fig. 7(a). Under the speeds of 10 and 20 m/s, the variation trend of wear rate is similar with the increase of load, whereas the rangeability at 10 m/s is bigger. At the sliding speed of 30 m/s, the wear rate increases slightly with increase in the normal load. The wear rate of Ti_2AlC is quite low and keeps in $(1.8–3)\times10^{-6}$ $mm^3/(N\cdot m)$. In the normal load range of 20–80 N, the wear rate of $Ti_2AlSn_{0.2}C$ increases as the sliding speed increases (see Fig. 7(b)), but it also can keep in a relatively low range of $(2–4)\times10^{-6}$ $mm^3/(N\cdot m)$. Compared with some ordinary ceramics such as Si_3N_4 (with a wear rate of $\sim10^{-4}$ $mm^3/(N\cdot m)$) [30] and PSZ (with a wear rate of $10^{-3}–10^{-2}$ $mm^3/(N\cdot m)$) [31], Ti_2AlC and $Ti_2AlSn_{0.2}C$ have much better abrasion wear resistance. Accordingly, we can add 0.2Sn or more to adjust the friction coefficient of the material within the range of 0.25–0.45, while it still maintains excellent wear resistance.

Typical SEM micrographs of the friction surfaces of Ti_2AlC and $Ti_2AlSn_{0.2}C$ after three continuous sliding processes performed under a normal load of 80 N and different sliding speeds are shown in Fig. 8 and Fig. 9, respectively. As shown, a thin film is adhered on the entire friction surface. When the sliding speed is at 10 m/s, the film is discontinuous, while the film is very uniform when the speed increases to 20 and 30 m/s.

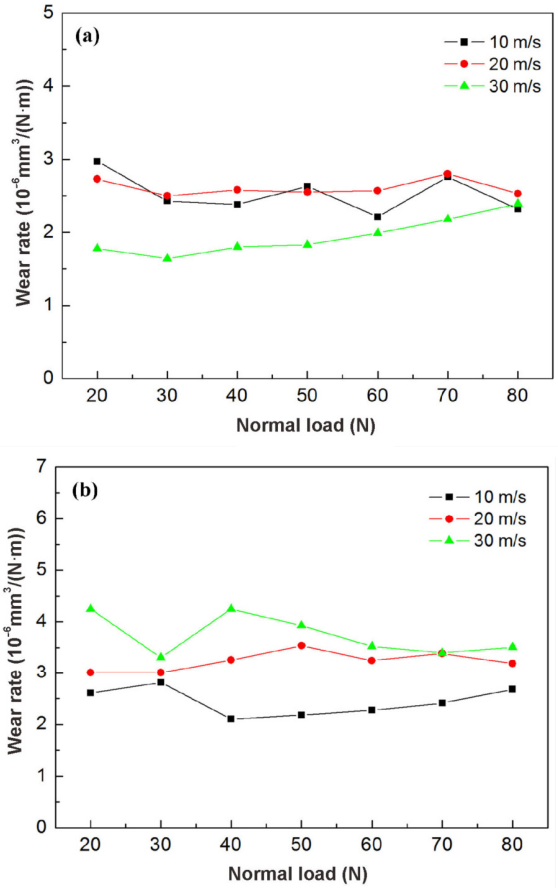

Fig. 7 Wear rates of (a) Ti_2AlC and (b) $Ti_2AlSn_{0.2}C$ sliding against low-carbon steel at different sliding speeds as a function of normal load.

EDS analyses were carried out to confirm the surface elements. It turns out that O, Ti, Al, and Fe can be detected in the friction surface of Ti_2AlC and a new element Sn can be detected in the friction surface of $Ti_2AlSn_{0.2}C$. Among them, Fe element comes from the low-carbon steel friction disk. EDS results show that the friction surface has the same elements, but at different contents. To further identify the phase behavior of fraction film, the XRD pattern was used. Figure 10 shows the XRD pattern of the $Ti_2AlSn_{0.2}C$ friction surface after sliding 36,000 m (three continuous processes) at 30 m/s and 80 N. From Fig. 10, some new phases can be observed compared to the original surface of $Ti_2AlSn_{0.2}C$ bulk (see Fig. 2), which are iron oxide, titanium oxide, tin oxide, and Al_2O_3, suggesting that the oxide frictional film is a combination of the oxides which can be corresponded with EDS result in Fig. 9.

Compared with the friction surfaces of Ti_2AlC and $Ti_2AlSn_{0.2}C$ in Fig. 8 and Fig. 9 respectively, it seems that the friction surface formed in the same friction test condition will be smoother after incorporating of 0.2Sn. It may be caused by the effect of tin oxide. In the oxidation behaviors of $Ti_2Al_{(1-x)}Sn_xC$ solid solution, SnO_2 is found to be formed at temperatures significantly lower than that of TiO_2 (rutile) and Al_2O_3 [15]. So tin oxide could be generated easier than titanium oxide and Al_2O_3, due to the local high temperature and pressure during the friction process. The mixed oxide film is responsible for the friction behavior as described in our previous work [9,10,22,23].

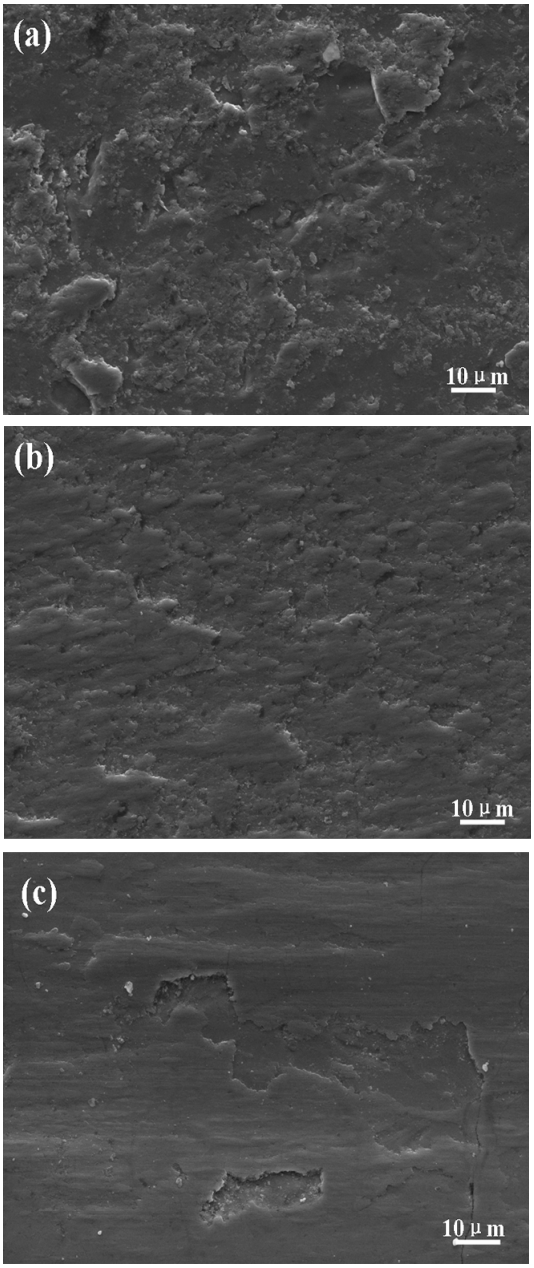

Fig. 8 Friction surface of Ti_2AlC bulk after sliding friction of (a) 10 m/s and 80 N, (b) 20 m/s and 80 N, (c) 30 m/s and 80 N.

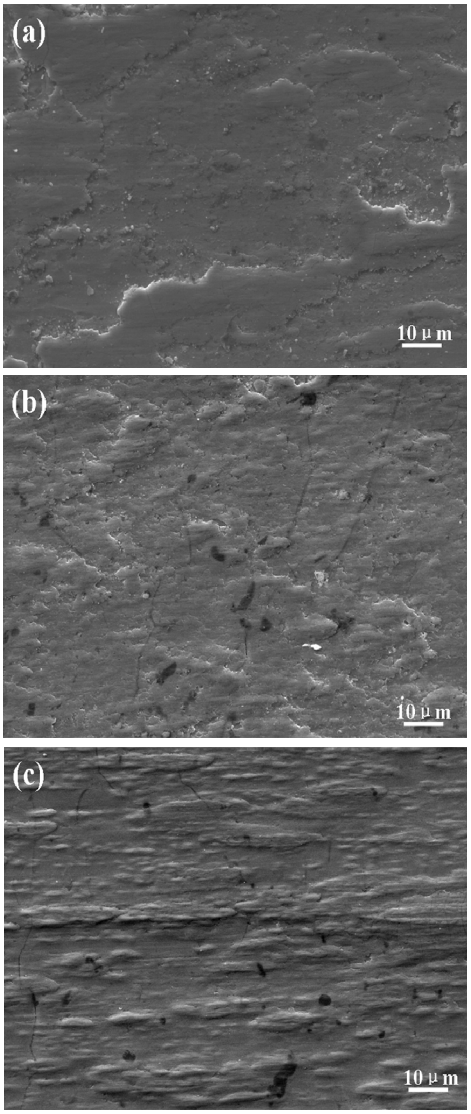

Fig. 9 Friction surface of $Ti_2AlSn_{0.2}C$ bulk after sliding friction of (a) 10 m/s and 80 N, (b) 20 m/s and 80 N, (c) 30 m/s and 80 N.

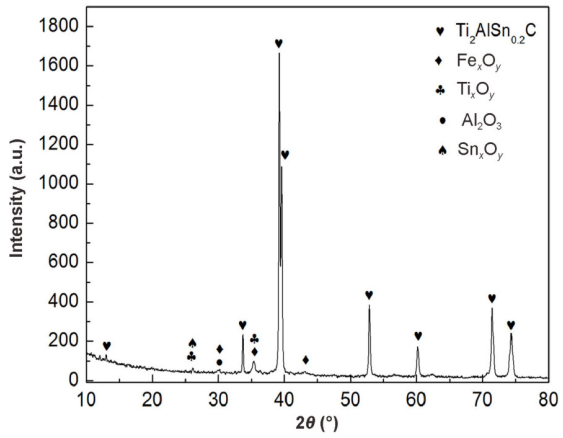

Fig. 10 XRD pattern of the $Ti_2AlSn_{0.2}C$ friction surface after 36,000 m (three continues processes) at 30 m/s and 80 N.

Sliding speed affects the coverage of friction surface oxide film. Huang *et al.* [23] have confirmed that a good oxide film with a higher percentage of coverage results in a smaller friction coefficient, and a poor oxide film with a lower percentage of coverage results in a larger friction coefficient. In the case of lower sliding speed of 10 m/s, the oxide film is lacked. When the sliding speed is higher at 20 and 30 m/s, the oxide film is continuous and smooth, the increased percentage of coverage results in the lower friction coefficient, and then the friction coefficients of Ti_2AlC and $Ti_2AlSn_{0.2}C$ decrease with increase in the sliding speed as Fig. 6 shows. In addition, the smoother friction surface of $Ti_2AlSn_{0.2}C$ results in lower friction coefficient and more stable friction behavior.

The wear rates of Ti_2AlC and $Ti_2AlSn_{0.2}C$ are also related closely with the existing oxide film. When lacking of the oxide film, the harder friction surface is at a severe wear stage between the low-carbon steel disk. With the increasing sliding speed, the instantaneous temperature of contact area rises, the softer oxide film is generated on the fraction surface, and the lubrication action of oxide film makes less wear rate. However, at the sliding speed of 30 m/s, when the normal pressure gradually increases, the oxide film flaking off results in higher wear rate. On the contrary, the wear pattern of $Ti_2AlSn_{0.2}C$ is different. Its oxide film is easier to form but also easier to peel. Simultaneously with the generating, the oxides would be consumed continuously from the friction surface. The more generated oxides result in the more consumed oxides, leading to the larger wear rate [23]. Furthermore, the wear rate of the material increases after adding 0.2Sn in Ti_2AlC, and this may be because that the frictional film with tin oxide on the $Ti_2AlSn_{0.2}C$ surface is combined loosely with the matrix and is easily stripped. So the wear rate is increased for $Ti_2AlSn_{0.2}C$.

El-Raghy *et al.* [20] have explored the macroscopic wear behavior of fine- and coarse-grained Ti_3SiC_2 samples. For both microstructures, there is an initial transition stage where the friction coefficient increases linearly from 0.15 to 0.45, and then rises to a steady state value of about 0.8. The stable period is longer for the fine-grained material. The average sliding wear rates are 4.25×10^{-3} and 1.34×10^{-3} $mm^3/(N\cdot m)$ for the fine- and coarse-grained samples, respectively. Delamination, crack bridging, grain buckling, microcracking, and grain fracture are energy-dissipating mechanisms believed to be responsible for the better wear resistance of the coarse-grained material

relative to the fine-grained material, where only grain pull out and fracture are observed. In our study, $Ti_2AlSn_{0.2}C$ with smaller grain size has lower friction coefficient and the value is stable, meanwhile it has a high wear rate. The results are well corresponding to the above literature, and maybe its friction mechanism can further explain the friction phenomenon in this particle. However, more work needs to be done in later experiments.

4 Conclusions

Ti_2AlC bulk with a little Ti_3AlC_2 has been synthesized by hot pressing at 1450 ℃ for 30 min with 28 MPa in Ar atmosphere, and a nearly pure, dense $Ti_2AlSn_{0.2}C$ solid solution was fabricated in the same condition. The solid solution hardening and strengthening effect was not observed after the incorporation of 0.2Sn. The flexural strengths of Ti_2AlC and $Ti_2AlSn_{0.2}C$ have been measured to be 430 and 410 MPa, respectively. Both Ti_2AlC and $Ti_2AlSn_{0.2}C$ had very low wear rates. The Sn incorporation in Ti_2AlC bulk resulted in the lower friction coefficient and more stable friction behavior, while a little higher wear rate. Experimental results showed that the friction surface with a layer of oxide film is responsible for the unusual tribological behaviors.

Acknowledgements

This work was supported by the Fundamental Research Funds for the Central Universities (Nos. 2016YJS122 and 2014JBZ015), the National Natural Science Foundation of China (NSFC, Nos. 51301013 and 51572017), and the Beijing Government Funds for the Constructive Project of Central Universities.

References

[1] Barsoum MW. The $M_{N+1}AX_N$ phases: A new class of solids: Thermodynamically stable nanolaminates. *Prog Solid State Ch* 2000, **28**: 201–281.

[2] Wang J, Zhou Y. Recent progress in theoretical prediction, preparation, and characterization of layered ternary transition-metal carbides. *Annu Rev Mater Res* 2009, **39**: 415–443.

[3] Wang XH, Zhou YC. Layered machinable and electrically conductive Ti_2AlC and Ti_3AlC_2 ceramics: A review. *J Mater Sci Technol* 2010, **26**: 385–416.

[4] Sun Z, Ahuja R, Schneider JM. Theoretical investigation of the solubility in $(M_xM'_{2-x})AlC$ (M and M′ = Ti, V, Cr). *Phys Rev B* 2003, **68**: 224112.

[5] Tian WB, Sun ZM, Hashimoto H, *et al.* Synthesis, microstructure and properties of $(Cr_{1-x}V_x)_2AlC$ solid solutions. *J Alloys Compd* 2009, **484**: 130–133.

[6] Chen JX, Zhou YC, Zhang J. Abnormal thermal expansion and thermal stability of $Ti_3Al_{1-x}Si_xC_2$ solid solutions. *Scripta Mater* 2006, **55**: 675–678.

[7] Zhou YC, Chen JX, Wang JY. Strengthening of Ti_3AlC_2 by incorporation of Si to form $Ti_3Al_{1-x}Si_xC_2$ solid solutions. *Acta Mater* 2006, **54**: 1317–1322.

[8] Li S-B, Bei G-P, Li C-W, *et al.* Synthesis and deformation microstructure of $Ti_3SiAl_{0.2}C_{1.8}$ solid solution. *Mat Sci Eng A* 2006, **441**: 202–205.

[9] Xu H, Huang Z, Zhai H, *et al.* Fabrication, mechanical properties, and tribological behaviors of $Ti_3Al_{0.8}Sn_{0.4}C_2$ solid solution by two-time hot-pressing method. *Int J Appl Ceram Tec* 2015, **12**: 783–789.

[10] Huang Z, Xu H, Zhai H, *et al.* Strengthening and tribological surface self-adaptability of Ti_3AlC_2 by incorporation of Sn to form $Ti_3Al(Sn)C_2$ solid solutions. *Ceram Int* 2015, **41**: 3701–3709.

[11] Bei GP, Gautheir-Brunet V, Tromas C, *et al.* Synthesis, characterization, and intrinsic hardness of layered nanolaminate Ti_3AlC_2 and $Ti_3Al_{0.8}Sn_{0.2}C_2$ solid solution. *J Am Ceram soc* 2012, **95**: 102–107.

[12] Dubois S, Bei GP, Tromas C, *et al.* Synthesis, microstructure, and mechanical properties of $Ti_3Sn_{(1-x)}Al_xC_2$ MAX phase solid solutions. *Int J Appl Ceram Tec* 2010, **7**: 719–729.

[13] Barsoum MW, El-Raghy T, Ali M. Processing and characterization of Ti_2AlC, Ti_2AlN, and $Ti_2AlC_{0.5}N_{0.5}$. *Metall Mater Trans A* 2000, **31**: 1857–1865.

[14] Barsoum MW, Tzenov N, Procopio A, *et al.* Oxidation of $Ti_{n+1}AlX_n$ (n = 1–3 and X = C, N). *J Electrochem Soc* 2001, **148**: C551–C562.

[15] Bei G, Pedimonte B-J, Fey T, *et al.* Oxidation behavior of MAX phase $Ti_2Al_{(1-x)}Sn_xC$ solid solution. *J Am Ceram Soc* 2013, **96**: 1359–1362.

[16] Bei GP, Pedimonte BJ, Pezoldt M, *et al.* Crack healing in $Ti_2Al_{0.5}Sn_{0.5}C$–Al_2O_3 composites. *J Am Ceram Soc* 2015, **98**: 1604–1610.

[17] Yu W, Li S, Sloof WG. Microstructure and mechanical properties of a $Cr_2Al(Si)C$ solid solution. *Mat Sci Eng A* 2010, **527**: 5997–6001.

[18] Ma J, Li F, Cheng J, *et al.* Tribological behavior of Ti_3AlC_2 against SiC at ambient and elevated temperatures. *Tribol Lett* 2013, **50**: 323–330.

[19] Gonzalez-Julian J, Llorente J, Bram M, *et al.* Novel Cr_2AlC MAX-phase/SiC fiber composites: Synthesis, processing and tribological response. *J Eur Ceram Soc* 2017, **37**: 467–475.

[20] El-Raghy T, Blaub P, Barsoum MW. Effect of grain size on friction and wear behavior of Ti_3SiC_2. *Wear* 2000, **238**: 125–130.

[21] Gupta S, Barsoum MW. On the tribology of the MAX phases and their composites during dry sliding: A review. *Wear* 2011, **271**: 1878–1894.

[22] Zhai H, Huang Z, Zhou Y, *et al.* Oxidation layer in sliding

friction surface of high-purity Ti_3SiC_2. *J Mater Sci* 2004, **39**: 6635–6637.

[23] Huang Z, Zhai H, Guan M, *et al.* Oxide-film-dependent tribological behaviors of Ti_3SiC_2. *Wear* 2007, **262**: 1079–1085.

[24] Lin ZJ, Zhuo MJ, Zhou YC, *et al.* Microstructural characterization of layered ternary Ti_2AlC. *Acta Mater* 2006, **54**: 1009–1015.

[25] Li S, Song G, Kwakernaak K, *et al*. Multiple crack healing of a Ti_2AlC ceramic. *J Eur Ceram Soc* 2012, **32**: 1813–1820.

[26] Meng FL, Zhou YC, Wang JY, *et al.* Strengthening of Ti_2AlC by substituting Ti with V. *Scripta Mater* 2005, **53**: 1369–1372.

[27] Zhou Y, Dong H, Wang X, *et al.* Preparation of Ti_2SnC by solid–liquid reaction synthesis and simultaneous densification method. *Mat Res Innovat* 2002, **6**: 219–225.

[28] El-Raghy T, Barsoum MW, Zavaliangos A, *et al*. Processing and mechanical properties of Ti_3SiC_2: II, Effect of grain size and deformation temperature. *J Am Ceram Soc* 1999, **82**: 2855–60.

[29] Salama I, El-Raghy T, Barsoum MW. Synthesis and mechanical properties of Nb_2AlC and $(Ti,Nb)_2AlC$. *J Alloys Compd* 2002, **347**: 271–278.

[30] Meng FY, Guo SY, Liu ZL, *et al.* Tribological characteristics of silicon nitride matrix ceramic. *Journal of Zhejiang Sci-Tech University* 2008, **25**: 79–82. (in Chinese)

[31] Tan Y, Wang Y, Rong X, *et al.* Study on friction and wear behavior of Mg-PSZ ceramics at different environmental temperatures. *Tribology* 1999, **19**: 337–341.